Nanotoxicology, 2011; Early Online, 1–13

ISSN: 1743-5390 print / 1743-5404 online
DOI: 10.3109/17435390.2011.626535

informa
healthcare

Length-dependent pathogenic effects of nickel nanowires in the lungs and the peritoneal cavity

Craig A. Poland[1,2], Fiona Byrne[3], Wan-Seob Cho[2], Adriele Prina-Mello[4], Fiona A. Murphy[2], Gemma Louise Davies[5], J.M.D. Coey[3], Yurii Gounko[5], Rodger Duffin[2], Yuri Volkov[4] & Ken Donaldson[2,6]

[1]Safenano, Institute of Occupational Medicine, Research Avenue North, Riccarton, Edinburgh, UK, [2]Centre for Inflammation Research, University of Edinburgh, Edinburgh, UK, [3]School of Physics and Centre for Research on Adaptive Nanostructures and Nanodevices (CRANN), Trinity College, Dublin 2, Ireland, [4]School of Medicine and CRANN, Trinity College, Dublin 2, Ireland, [5]School of Chemistry and CRANN, Trinity College, Dublin 2, Ireland and [6]Institute of Occupational Medicine, University of Edinburgh, Research Avenue North, Riccarton, Edinburgh, UK

Abstract

The use of fibre-shaped nanomaterials in commercial applications has met with concern that they could cause health effects similar to those seen with pathogenic fibres such as certain forms of asbestos. Of the attributes which form the fibre pathogenicity paradigm, fibre length is thought to be a critical factor in determining fibre toxicity. We have previously shown that carbon nanotubes display such length-dependent pathogenicity but it remains unclear if other forms of fibrous nanomaterials conform to the fibre pathogenicity paradigm. As such, our aim is to determine the generality of this hypothesis by asking whether a radically different form of fibrous nanomaterial, nickel nanowires, show length-dependent pathogenicity. Our results indicate that nickel nanowires synthesised to be predominantly long (>20 μm) show the ability to elicit strong inflammation in the mouse peritoneal model in a dose-dependent manner; inflammation or fibrosis was not seen with the short (<5 μm) nanowires. This length-dependent response was also seen after lung aspiration and within a macrophage *in vitro* model adding further weight to the contention that fibre length is an important driver of hazard potential. This may have important implications when considering the hazard posed by fibrous nanomaterials and their regulation in workplaces.

Keywords: Nanofibres, fibre pathogenicity paradigm, inflammation, structure activity relationship

Introduction

Fibres have long been used as an industrial material due to commercially advantageous properties such as tensile strength and anisotropic electrical or thermal conductivity. However, the experience with asbestos, a fibrous silicate mineral, engendered a general suspicion that industrial fibres are pathogenic and this suspicion has fallen on new forms of engineered nanofibres currently being developed. However, the large variety of industrial fibres display a wide range of toxicities from, in the majority of cases, harmless fibres to those which cause a variety of diseases including cancer. Knowledge regarding the toxicity of a wide variety of pathogenic and non-pathogenic fibres, such as asbestos, led to the development of a fibre pathogenicity paradigm (FPP) through the work of such luminaries as Stanton (Stanton et al. 1981) and Pott (Pott et al. 1987) and as discussed recently in relation to the organic fibre para-aramid (Donaldson 2009) and in relation to carbon nanotubes (CNTs) (Donaldson et al. 2010). The FPP is based on three essential physicochemical attributes which a fibre must possess to be pathogenic in a fibre-specific manner. These are: diameter less than 3 μm to allow aerodynamic penetration into the lung; a length greater than approximately 15 μm to frustrate macrophage mediated clearance; and resistance to dissolution and/or breakage in the biological environment causing the fibre to persist – biopersistence (Donaldson 2009). The suggestion that fibrous nanomaterials might conform to the FPP was first raised in relation to CNTs (Service 1998; The Royal Society and Royal Academy of Engineering 2004). CNTs by virtue of their nano and graphenic nature are thin and biopersistent, but can vary considerably in length. Long CNTs therefore can fulfil all the attributes of a pathogenic fibre, if long, and have been shown to be both highly inflammogenic and fibrogenic in the peritoneal cavity in this form (Poland et al. 2008). This raises the question which forms the basis of this study: do other nanofibres show length-dependent toxicity?

Through the commercialisation of nanoparticles (NPs) and their incorporation into an ever more diverse range of products and applications, engineered NPs are increasingly becoming part of today's world. This has raised the

Correspondence: Craig Poland, Safenano, Institute of Occupational Medicine, Research Avenue North, Riccarton, Edinburgh EH14 4AP, Tel: +44(0)131 449 8096. Fax: +44(0)131 449 8084. E-mail: craig.poland@iom-world.org

(Received 21 March 2011; accepted 23 August 2011)

increasing likelihood of exposure of those working with NPs in the occupational setting and also ultimately the end-users of NP containing products as these undergo attrition and wear. Such exposures have potential to produce adverse health consequences (Maynard et al. 2006; Donaldson et al. 2006). Whilst CNTs are the most well known of the nanofibres, others are also under development for commercial application. Of the various methods which continue to be developed for the production of nanowires, the use of template-based growth methods is becoming increasingly popular (Figure 1). Part of the reason for the interest in nanowires is the controllability of the production process including diameter, length and density, reduced contamination as well as low production costs and easy scalability (Cao & Liu 2008). Template-based systems make use of nano-scale templates into which a material of choice is deposited, leading to the self assembly of a nanowire followed by recovery of the nanofibres from the template. Templates can consist of wide range of substrates, most often alumina membranes (Prina-Mello et al. 2006) but even nano-biological structures such as the tobacco mosaic virus (Knez et al. 2003) or microtubules (Zhou et al. 2008) can be used. Whilst nanowires differ from CNTs in commercially desirable traits such as tensile strength, the commercial interest in nanowires is likely to increase in the coming years. The nickel nanowires (NiNWs) used within this study are very different from CNT or asbestos fibres and represent an ideal candidate to test an alternative form of high aspect ratio nanoparticles (HARN) against the FPP. As such, our aim is to ascertain if this different form of HARN also shows length-dependent pathogenicity in a model of direct mesothelial exposure.

Materials and methods

Our approach was the development of long nickel nanowires (L-NiNW) and short nickel nanowires (S-NiNW) to allow the critical evaluation of the length hypothesis and its contribution to the toxicity of a fibre. These samples were evaluated for their potency in eliciting both inflammogenic and fibrogenic activity in a model of direct mesothelial exposure using the mouse peritoneal assay. In addition, we explored the differential toxicities of these materials within the lung and also if an *in vitro* model (THP-1 cells) could be used to differentiate between toxicity driven by fibre length.

NiNW fabrication and characterisation

NiNWs were fabricated by electrochemical template synthesis (Figure 1) using alumina membranes (Anodisc 25, Whatman, UK) with an average pore diameter of 200 nm, as reported in our previous work (Prina-Mello et al. 2006; Byrne et al. 2009). Nanowires were removed from the membrane by dissolving it in 1 M NaOH and re-suspending the solution in deionised water. The metallic NiNWs due to oxidation possessed a 3–4 nm layer of nickel oxide over the surface (Prina-Mello et al. 2006). S-NiNW and L-NiNW with average lengths of 4.3 ± 1 μm and 24 ± 7 μm were examined and sized by counting a minimum of 100 separate

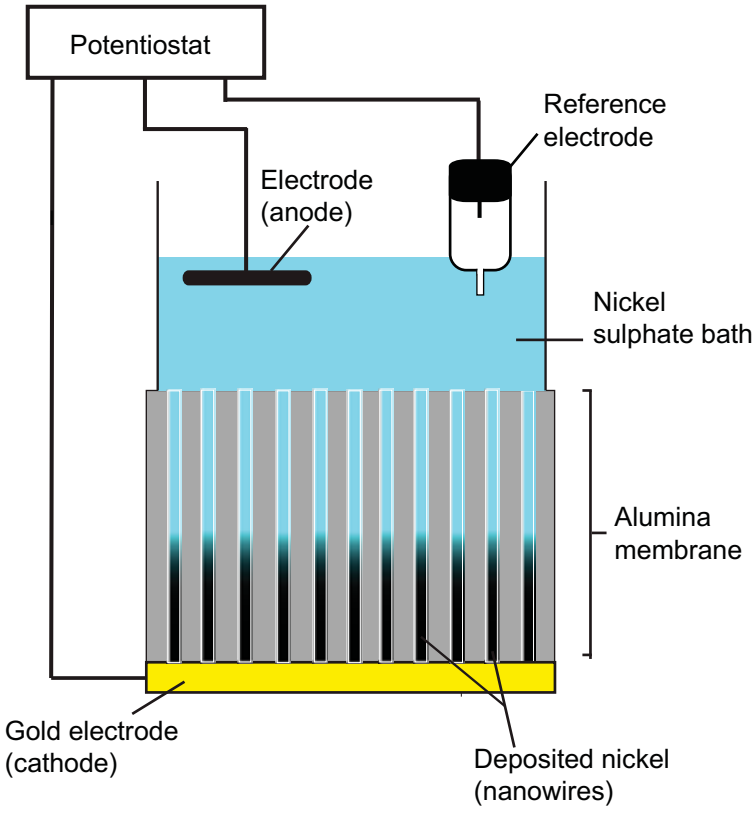

Figure 1. Diagram of nickel nanowire synthesis. The typical template mechanism for the production of nickel (and other electrically conductive material) nanowires is shown (adapted from Cao & Liu 2008).

nanowires scanning electron microscopy (Carl Zeiss Ultra Plus, UK). In order to control for bulk chemical composition, we utilised a commercially available nickel nanoparticle (NiNP) (Nanostructured & amorphous materials Inc., TX, USA). These particles were non-fibrous and spherical in shape, with a mean dry particle diameter of 15 nm (±5 nm; manufacturer's description) and a hydrodynamic diameter of 57 (±10) nm in experimental dispersant (0.5% bovine serum albumin (BSA) (Sigma-Aldrich, Poole, UK)/saline), ascertained by diffraction light scattering (Brookhaven Instruments Corporation, NY, USA).

Particle suspension

All particles were suspended in a solution containing 0.5% w/v BSA. For *in vitro* experiments, the solution consisted of Rosewell Park Memorial Institute-1640 (RPMI-1640) cell culture media (PAA Laboratories Ltd., UK) supplemented with 100 U/ml penicillin/streptomycin and 2 mM of L-Glutamine (PAA Laboratories Ltd., UK). For *in vivo* experiments, 0.5% BSA was added to sterile saline suitable for injection. Once dissolved, the BSA solution (media/saline) was sterile filtered using a 0.22 μm filter (Whatman, UK) to remove any contamination and large globular proteins and used immediately. Each particle type was made up in the BSA surfactant and sonicated in a sealed container using an ultra-sonicating water bath (Fisherbrand FB11002, 40 kHz, UK) for 2 h to achieve a visually homogenous suspension. The samples were then diluted to the appropriate test concentrations with the BSA surfactant and briefly sonicated to ensure proper mixing.

Experimental animals

Eight to twelve week old (20–25 g) female C57BL/6 strain mice (Harlan, UK) were group housed in standard caging with sawdust bedding, environmental enrichment with free access to sterile water and food within a pathogen-free Home Office approved facility. The animals were maintained on a normal 12 h light and dark cycle and were allowed 7 days to acclimatise prior to study commencement. Post exposure animals were subject to daily checks for signs of distress or welfare issues (none identified). All *in vivo* work was carried out by staff holding a valid UK Home Office personal licence under a Home Office approved project licence.

Intraperitoneal injection

After 7 days acclimatisation, groups of three animals were injected intraperitoneally with 0.5 ml of 100 μg/ml (50 μg/animal) of each particle treatment or 0.5 ml of 0.5% BSA/saline as a vehicle control. Animals were immediately placed back into their cage and monitored to ensure resumption of normal behaviour. The animals were sacrificed at 24 h to investigate the acute inflammatory effects or 7 days for investigation of the inflammatory and fibrotic effects.

At each time point, the mice were sacrificed by CO_2 asphyxiation or cervical dislocation and the peritoneum lavaged three times using 2 ml washes of sterile ice-cold saline. Three washes were shown to be sufficient to allow the removal of 90% of free floating peritoneal cells by exhaustive lavage (data not shown). The lavages were pooled together and placed on ice for the entire duration of the processing.

Pharyngeal aspiration

Animals were anesthetised using isoflurane (2-chloro-2-(difluoromethoxy)-1,1,1-trifluoro-ethane) and the tongue was gently held at full extension and a 50 μl bolus of test sample pipetted to the base of the tongue. The animals were stimulated to inhale via covering of the nasal cavities to induce a gasp reflex and held until several breaths had occurred (Rao et al. 2003). The animals were further observed until full recovery and group housed for the duration of the experiment.

At each time point, the mice were sacrificed by terminal anaesthesia using an intraperitoneal injection with 0.5 ml of pentobarbitone (200 mg/ml) followed by exsanguination via the abdominal aorta. The thoracic cavity was exposed, and the trachea cannulated using a 21 gauge needle and ligated. The lungs were lavaged using three 1 ml washes of ice-cold sterile saline with the first lavage retained separately and the subsequent lavages pooled. All lavages were placed on ice for the entire duration of the processing.

Dissection and fixation

Diaphragm

Following sacrifice and peritoneal lavage the abdominal wall of the animal was removed, exposing the peritoneal cavity. Lateral incisions extending to the veterebral column were made, which was then severed below the diaphragm and the diaphragm carefully removed by cutting through the chest wall approximately 1 cm from the diaphragm. The diaphragm was rinsed three times by emersion in ice-cold sterile saline and placed overnight into methacarn fixative (60% methanol, 30% chloroform and 10% glacial acetic acid) for histological staining. After overnight incubation in fixative, the diaphragm was carefully excised from the surrounding ribs and the same full width section of the upper (ventral) portion of the diaphragm removed from each animal sampled. As previously described (Poland et al. 2008), the diaphragm sections were dehydrated through graded alcohol (ethanol) and imbedded on-edge in paraffin, with 4 μm sections of the diaphragm made and stained with haematoxylin and eosin (H&E) stain. Serial images were taken at ×100 magnification along the diaphragm length using QCapture Pro software (Media Cyberbernetics Inc., MD, USA) and seamlessly re-aligned using Adobe Photoshop CS3 Version: 10.0.1 (Adobe systems Inc.) to show the entire diaphragm section. Using calibrated software (Image-Pro Plus, Media Cybernetics Inc., MD, USA), the total length of each diaphragm along the basement membrane was measured in order to adjust for any differences in size between diaphragms. Any areas of granulomatous tissue, identified by histology as lymphocytic aggregates adhering to the diaphragm surface (excluding areas of Liver, connective tissue or lymphatic tissue), were measured using the same software. Granuloma area on each diaphragm was calculated in mm^2 per unit length of diaphragm (in mm) to yield

granuloma area per unit diaphragm length (mm^2/mm) as shown in Figure 5.

Lung

At each time point, the mice were sacrificed by terminal anaesthesia, the lungs exposed and the trachea cannulated as before. The heart and lungs were removed on-block and fixed by instillation of a cold methacarn fixative at a hydrostatic pressure of 20 cm H_2O. The entire lung was submerged in fixative for a period of 24 h prior to processing. After fixation, the heart was removed and discarded whilst the individual lobes of the lung were dissected free and placed flat in a tissue cassette. As before, the lung tissue was dehydrated through graded alcohol (ethanol) and imbedded in paraffin with four sections cut so as to encompass all lobes of the lung. Sections were stained with H&E stain to show gross pathology and Pico-Sirius Red to show collagen deposition (red stain) and serial images taken at ×100 magnification using QCapture Pro software (Media Cyberbernetics Inc., MD, USA). The images were seamlessly re-aligned using Adobe Photoshop CS3 Version: 10.0.1 (Adobe systems Inc.) to show the entire section of the lung.

Differential cell count

The lavage fluid (both lung and peritoneal) was then centrifuged at 123 g for 5 min at 4°C in a Mistral 3000i centrifuge (Thermo Fisher Scientific, Inc., MA, USA) and aliquot of the supernatant retained for total protein and cytokine measurements. The remaining cell pellet was re-suspended in 0.5 ml of 0.1% BSA/sterile saline solution. A total cell count was then performed using a NucleoCounter (ChemoMetec, A/S, Allerød, Denmark). Differential cell counts were performed on cyto-centrifugation preparations, stained with Diff Quik. Images of cells were taken using QCapture Pro (Media Cyberbernetics Inc., MD, USA).

Total protein measurements

Total protein concentration of the peritoneal lavage fluid was measured using the bicinchoninic acid protein assay. Sample protein concentrations were established by comparison to a BSA standard (Sigma-Aldrich, Poole, UK) curve

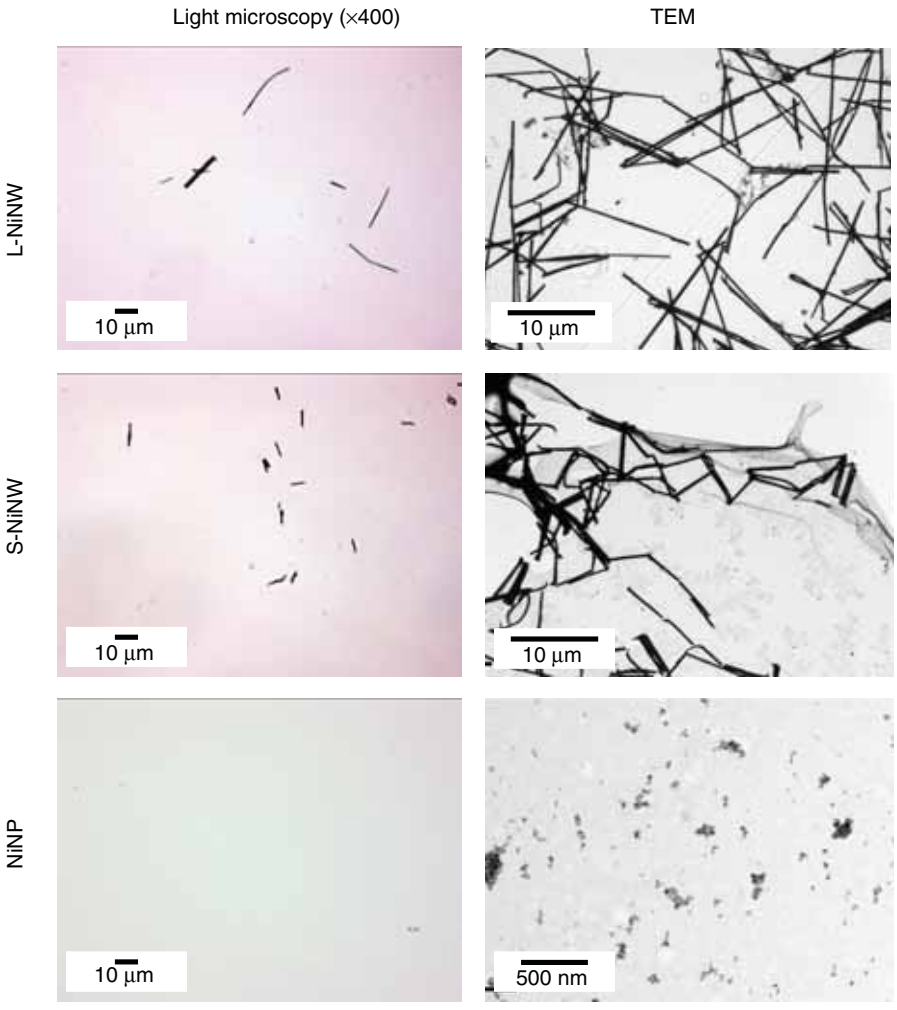

Figure 2. Morphological structure of nickel nanowires (NiNW) and nickel nanoparticles (NiNP). Brightfield images of nickel based nanoparticles were taken at ×400 magnification in glycerol after dispersion in dH_2O (left hand panel). TEM images were taken for NiNP dispersed in dH_2O and deposited onto formvar coated TEM grids (0.5 µg) prior to imaging. (Right hand panel) (Please note the different scale bar between TEM of NiNW and NiNP).

(0–1000 μg/ml). The samples were then incubated at 37°C for 30 min after the addition of the test reagent (1 part Cu II sulphate solution (4% w/v) to 50 parts bicinchoninic acid (Sigma-Aldrich, Poole, UK)). The absorbance was then read at 570 nm using a Synergy HT microplate reader (BioTek Instruments, Inc. VT, USA) and the sample protein concentration established via derivation from the BSA standard curve.

LDH assay

The level of cellular cytotoxicity/cytolysis was established using a lactate dehydrogenase (LDH) assay (Roche Diagnostics GmbH, Mannheim, Germany). Briefly, 100 μl of lavage fluid was added in triplicate to a 96-well plate and 100 μl of the LDH test reagent (diaphorase/NAD^+ mixed with iodotetrazolium chloride and sodium lactate at a ratio of 1:45) added to each well. Following a 30 min incubation period, the absorbance of each well at 490 nm wavelength was established using a Synergy HT microplate reader (BioTek Instruments, Inc. VT, USA).

THP-1 cell culture

The monocytic cell line THP-1 was obtained from the American Type Culture Collection and maintained at subculture in RPMI-1640 supplemented with 10% foetal calf serum (PAA Laboratories Ltd., UK) at 37°C (4% CO^2). Cells were differentiated from their monocytic form into macrophage-like cells via 24 h incubation with 5 μM of phorbol myristate acetate (PMA; Sigma-Aldrich, Poole, UK). Briefly, THP-1 cells were seeded into 24-well plates at a density of 1 million cells/ml (0.5 ml total volume) and incubated with 5 μM of PMA for 24 h triggering differentiation and causing the cells to become adherent. Any non-adherent cells were removed and the media replaced with fresh 2% FCS containing media for 24 h. The seeded cells were then exposed for 24 h to the different lengths of NiNPs at a concentration of 5 μg/ml. After 24 h an aliquot of the media supernatant retained for cytokine analysis, the remaining supernatant aspirated, the cells stained with Diff Quik stain and images of cells were taken using QCapture Pro (Media Cyberbernetics Inc., MD, USA).

Cytokine/chemokine assay

The media levels of interleukin-1β (IL-1β), interlukin-6 (IL-6), tumour necrosis factor-alpha (TNF-α) and the chemokine CCL3 (MIP-1α) were established using ELISA Duo-Set kits (R&D systems, Abingdon, UK) specific to each analyte of interest. Ninety-six well microtitre plates (Corning) were incubated overnight at 4°C with 100 μl coating antibody raised against IL-1β, IL-6, TNF-α or CCL3. The plates were washed three times with 0.05% Tween-20 in phosphate buffered saline (PBS; pH 7.2) and blocked using reagent diluent (1% BSA in PBS; R&D systems, Abingdon, UK) for 1 h (room temperature) prior to further washing and addition of test samples/standards in triplicate. After 2 h, the plates were washed and a biotinylated detection antibody added to each well followed by a further 2 h incubation, followed by washing and the addition of HRP conjugated streptavidin. The plates were washed and developed using a TMB substrate solution (Sigma-Aldrich, Poole, UK). The subsequent reaction was stopped with 0.5 M H_2SO_4, resulting in a yellow colour, and read at 450 nm. Sample concentrations of IL-1β, IL-6, TNF-α and CCL3 were established via extrapolation from the appropriate recombinant protein standard curve.

Statistical analysis

All data were analysed using GraphPad Prism 5 (Version 5.03; GraphPad Software Inc. USA). Results were expressed as the mean + standard error mean (s.e.m) and multiple comparisons were analysed using one-way analysis of variance with a Tukey-HSD method post-test. Two sample comparisons were made using the Student's *t*-test. In all cases, values of $p < 0.05$ were considered significant.

Results

Particle characterisation

By altering the deposition time in the fibre-production process, the length of the nanowires was altered allowing the formation of a predominantly long (L-NiNW) and a predominantly short test sample (S-NiNW) as shown in Figure 2.

The L-NiNWs were predominantly (73%) above 20 μm in length (Figure 3) with a mean length (± standard deviation) of 24 μm (±7 μm) and hence given the notation L-NiNW. The second nanowire sample used was a short fibre sample with 100% of the fibres less than 10 μm and 77% less than 5 μm in length (Figure 3) with a mean fibre length of 4 ± 1 μm, denominated S-NiNW. The TEM image shown in the right hand panel of Figure 2 shows the short fibres forming disjointed end-on chains (dipole–dipole interaction between NiNWs due to their remnant magnetisation); these are

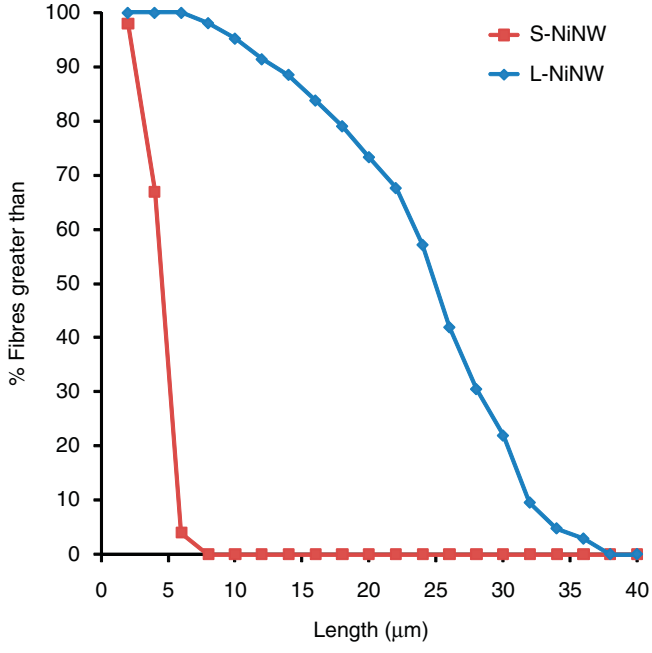

Figure 3. Nickel nanowire size distribution. Size distribution was performed by measurement of a minimum of 100 fibres imaged under scanning electron microscopy (SEM, Carl Zeiss Ultra Plus, UK).

readily dispersed into singlet short fibres in protein solution for injection as shown under the light microscopy images in the left hand panel. All of these fibres irrespective of length had straight morphology and regular diameter of 200 ± 10 nm.

Sonication of the NiNW samples during dispersion for *in vivo*/*in vitro* use did lead to a small degree of shortening. Subsequent control experiments using a separate batch of NiNWs demonstrated that a 2 h sonication using an ultrasonicating water bath induced a 7% and a 4% decrease in the long and short samples, respectively (data not shown). This therefore suggests that whilst marginal shortening did occur, the resultant fibres still met the minimal and maximal length requirements of the experimental design for the long and short fibres respectively as reflected in Figure 2 (light microscopy image).

Length-dependent fibre toxicity

Twenty-four hours after injection of 50 µg of L-NiNW (~7.9×10^6 fibres), S-NiNW (~31.25×10^6 fibres) and NiNP into the peritoneal cavity, the inflammatory response to each particle was evaluated following washing (lavaging) the peritoneal cavity with ice-cold sterile saline. The total number of inflammatory neutrophils (Polymorphonuclear leukocyte; PMN), a potent marker of acute inflammation, and total protein levels within the lavage fluid as a measure of increased vascular permeability due to inflammation was established (Figure 4A). The results demonstrate a highly significant increase with L-NiNW ($p < 0.001$) compared to controls, which is significantly greater than that of S-NiNW and NiNP ($p < 0.001$). Figure 4B shows the typical cellular response post injection with the S-NiNW (top panel) and NiNP (bottom panel) showing complete unperturbed uptake of the particles by macrophages. Uptake of the L-NiNW sample (middle panel) is associated with frustration of the process of phagocytosis by failure to fully enclose the fibre. This leads to an inflammatory cell influx as noted by the presence of neutrophils in the lavage fluid.

Figure 5 shows the response at the diaphragmatic mesothelial surface 7 days post injection with the two NiNWs and control NPs, the point of fibre egress and hence deposition of the long fibres. Treatment with S-NiNW or the compact NiNP control showed no lesions on the peritoneal aspect of the diaphragm at the mesothelium. In contrast, treatment

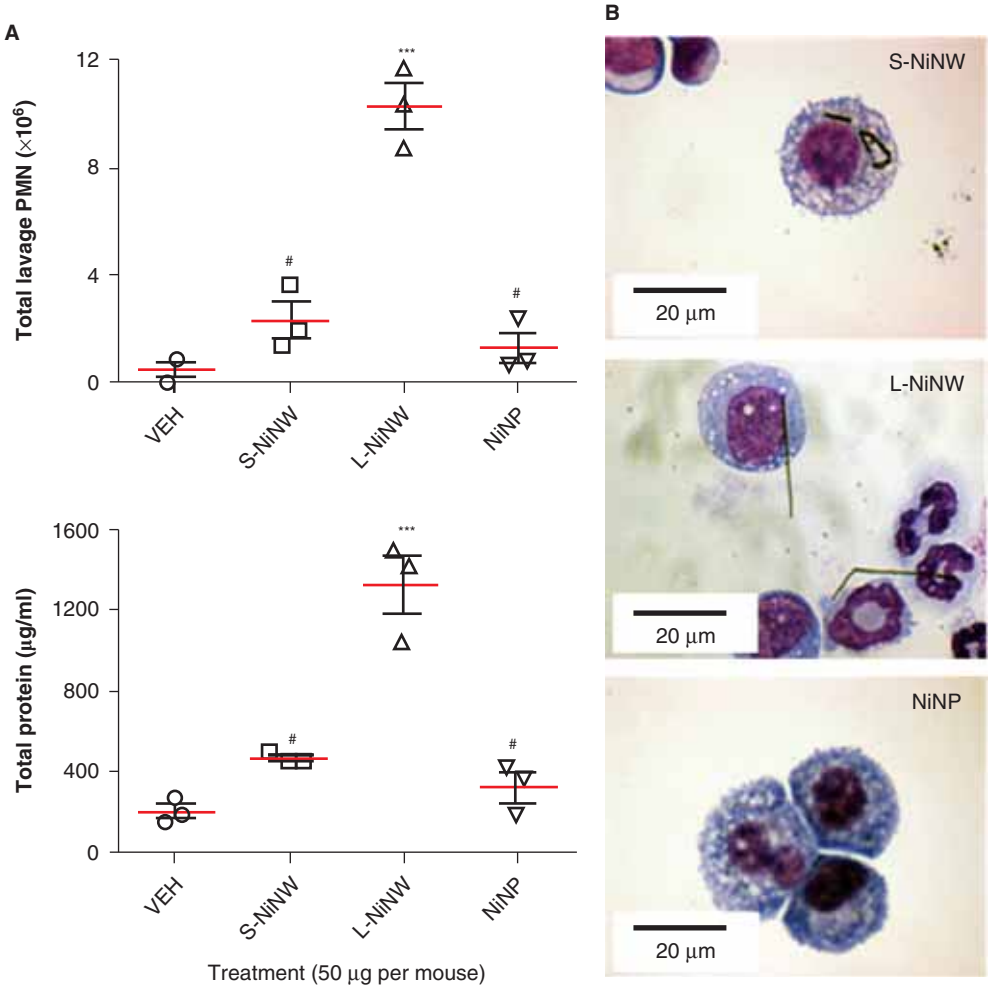

Figure 4. Length-dependent inflammogenicity of nickel nanowires. (A) Female C57BL/6 mice were intraperitoneally injected with 50 µg of long (L-NiNW) and short (S-NiNW) nickel nanowires and the peritoneal cavity lavaged 24 h later to assess the level acute inflammation. Panel B shows typical macrophage uptake of NiNW and nanoparticles in the peritoneal cavity 24 h after injection. Scatter plot with mean of three animals ± s.e.m. Significance vs. vehicle control indicated by $p < 0.001$ and vs. L-NiNW $^{\#}p < 0.001$. All images were taken at ×1000 magnification under Brightfield illumination.

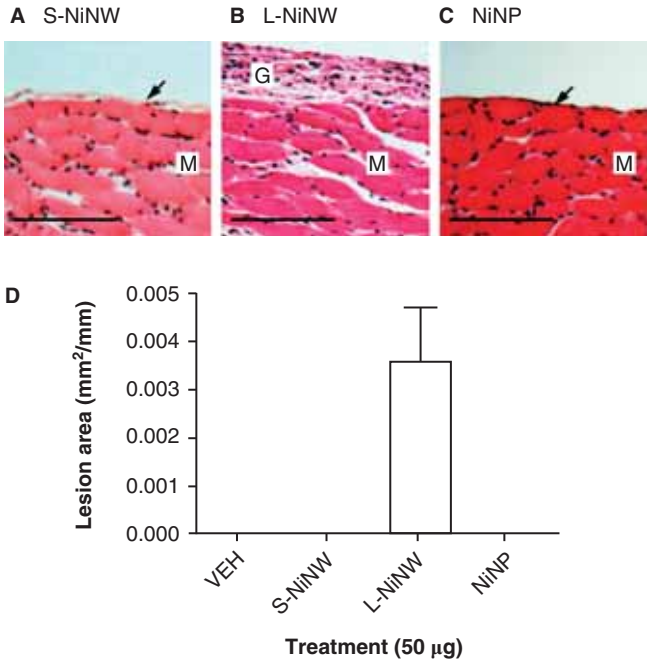

Figure 5. Granulomatous response post injection with long (L-NiNW) but not short nickel nanowires (S-NiNW) or nanoparticles. C57BL/6 mice were intraperitoneally injected with 50 μg of S-NiNW (A) or L-NiNW (B) nickel nanowires and nickel nanoparticle (NiNP; C). Seven days post injection the animals were sacrificed and the diaphragm removed and sectioned for histological examination for the presence of granulomatous lesions. The peritoneal aspect of the diaphragm is shown with the muscular area (M) and overlying mesothelium (arrow) shown. Areas of granuloma (G) are shown and were measured and expressed per millimeter of the total section length (D). Mean of three animals (for vehicle control, S-NiNW, NiNP exposure) and six animals (for L-NiNW exposure) ± s.e.m.

with L-NiNW resulted in granulomas at the mesothelial surface.

To investigate the dose-relatedness of inflammogenicity of the L-NiNW, mice were injected intraperitoneally at mass doses of 0.5, 1, 10 and 50 μg per mouse in a 0.5 ml vehicle of 0.5% BSA/saline and the peritoneal cavity lavaged 24 h later. Injection of L-NiNW into the peritoneal cavity of C57BL/6 mice led to an induction of a straight-line dose response relationship for neutrophil infiltration ($r^2 = 0.9863$; Figure 6). This response at 50 μg per mouse was in excess of what we have previously seen with the same mass of long multi-walled CNT and long fibre amosite asbestos (Poland et al. 2008); total protein levels in the peritoneal lavage fluid at 24 h supported the PMN data. Injected animals were also lavaged at 7 days post injection to show chronicity of the inflammation (Figure 6; right hand panel). However, after 7 days the inflammatory response was markedly reduced showing no dose–response relationship and only a dose of 1 μg of NiNW per mouse produced a significant increase in neutrophil influx over vehicle control.

We excluded a role for soluble agents leaching from the particle surface in these effects by using an aqueous extract which is a commonly used methodology to collect soluble metals from particle samples (Brown et al. 2000; Cho et al. 2011; McNeilly et al. 2004) and assessed their role in adverse effects. This was prepared by 24 h mixing of the highest dose of L-NiNW (50 μg) in sterile saline without biological macromolecules as is commonly the case in many studies by other groups (Hetland et al. 2001; Knaapen et al. 2002) and forms the basis of a recommended methodology for studying the soluble bio-available components of particles (Julien et al. 2011). This was followed by centrifugation to remove the long nanowires and which would have contained any soluble Ni ions or other soluble components. Soluble components are known to play a role in the toxicity of combustion derived NPs (Nel et al. 2001; McNeilly et al. 2004) and other metallic NPs such as Cu and Zn (Cho et al. 2011) but the lack of inflammation after instillation of the aqueous extract (Appendix Figure 1) confirmed that nickel ions did not contribute to the inflammogenicity of the L-NiNW sample.

In addition to the mesothelioma hazard, which we studied here by examining the short-term mesothelial inflammatory response to the NiNW, fibres also pose a hazard to the lungs in the form of fibrosis and lung cancer. We assessed this by aspirating 50 μg of L-NiNW and S-NiNW and NiNP into the lungs of mice (Figure 7).

As NiNPs are known to be inflammogenic in the lung (Lu et al. 2009), we expected an inflammatory reaction with all forms of nickel aspirated into the lungs but we also expected an enhanced response and characteristic pathology due to long fibres and the clearance problems that they pose to macrophages as described above. This was confirmed by the presence of elevated BAL PMN in all nickel exposed groups compared to vehicle control group (Appendix Figure 2). However, there was a dramatic difference in pathological response between the nickel particle types at 7 days. This was most evident in the comparison between the NiNP and the long L-NiNW. The presence of NiNP caused a very mild diffuse alveolitis as would be expected by the NiNP reaching the alveolar region following instillation. However, there was no remodelling or fibrosis of the airways and only mild alveolar wall thickening at sites of inflammation although there were very occasional instances of small granulomas with mild collagen staining around larger aggregates of NiNPs (not shown). Deposition of L-NiNW in contrast led only to a moderate inflammatory response in the peripheral airways (Figure 8, Appendix Figure 2) but did lead to a strong granulomatous response evident as areas of intense nuclear staining in solid, highly cellular granulomas (Figure 7C). These granulomas consisted of macrophages and numerous NiNW fibres. Due to the shorter size of the s-NiNW, retention did not occur predominantly at the terminal bronchioles and particles reached the alveolar region with subsequent alveoli wall thickening rather similar to what was seen with NiNP. Figure 8 shows representative images of the alveolar septae taken at equidistance from the terminal bronchioles and shows that both L-NiNW and S-NiNW generated thickening of the alveolar septae to a similar degree.

In vitro toxicity of long fibres

An *in vitro* exposure method was developed to investigate long and short fibre effects. We used the monocytic leukaemia cell line THP-1, which was further differentiated into macrophages using PMA. The differentiated

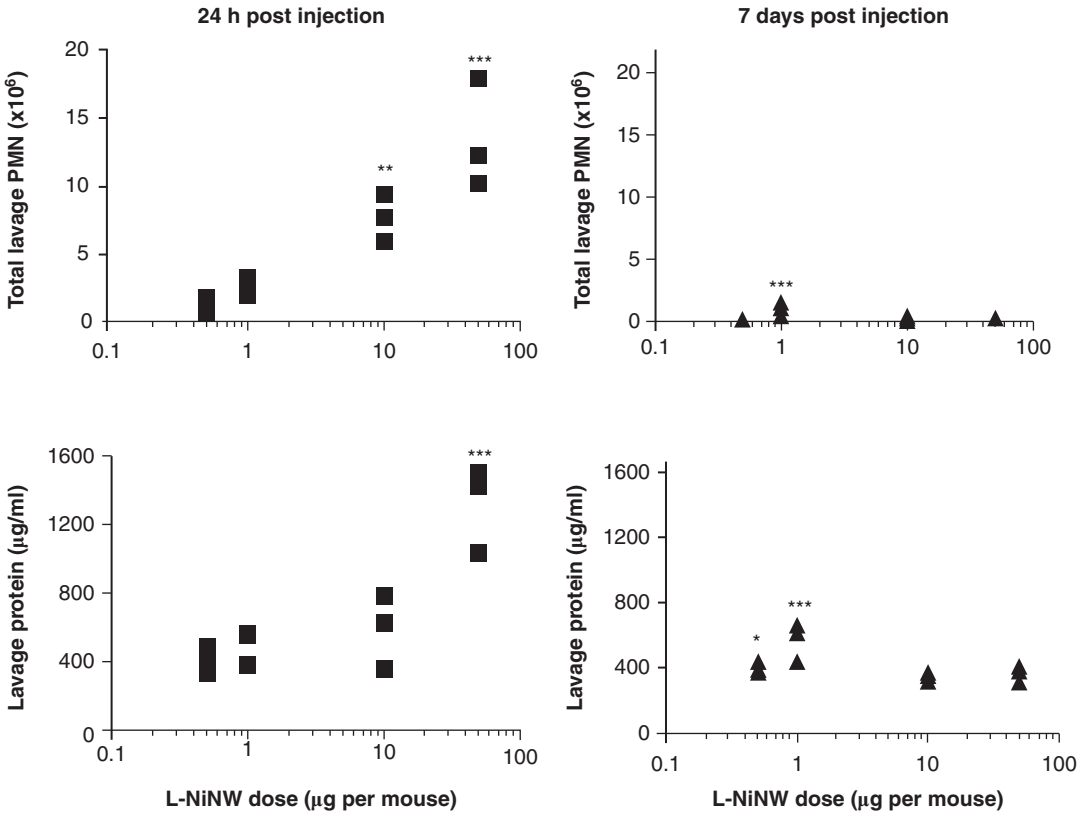

Figure 6. Inflammatory response post intraperitoneal injection with long nickel nanowires (L-NiNW). Female C57BL/6 mice were intraperitoneally injected with increasing doses of L-NiNW and 24 h or 7 days post injection were sacrificed and the peritoneal cavity lavaged. Total lavage neutrophil (Polymorphonuclear leukocyte (PMN)) numbers were counted (top graphs) and total lavage protein measured as a general marker of inflammation (bottom graphs). Mean of three animals ± s.e.m. Significance vs. vehicle control indicated by $^{*}p < 0.05$, $^{**}p < 0.01$ and $^{***}p < 0.001$.

THP-1 cells were exposed for 24 h to the different lengths of NiNPs and their responses analysed. As shown in Figure 9, secretion of the acute phase response cytokines IL-1β and IL-6 followed the pattern seen *in vivo* in the peritoneal cavity with long and short nanowires and NiNP. In these cases, a significant increase in both cytokines was seen after treatment with L-NiNW ($p \leq 0.001$) over vehicle control and the S-NiNW and NiNP. Length-dependent effect of the L-NiNW was seen with TNF-α and the chemokine CCL3 (MIP-1α) but NiNP also significantly increased levels of TNF-α and CCL3.

Cytocentrifugation preparations after treatment with S-NiNW (Figure 9E) and L-NiNW (Figure 9F) show cellular uptake of the particles. In the case of L-NiNW, fibres can be seen both within and protruding out of the macrophages whilst the S-NiNW were completely enclosed (as shown by arrows).

Discussion

Our intention within this series of experiments was to ascertain if a radically different form of HARN to CNTs also show length-dependent pathogenicity in a model of direct mesothelial exposure and a surrogate for the thoracic cavity. Using a compositionally and structurally different form of HARN, we report here that, similar to asbestos and CNTs (Poland et al. 2008; Donaldson et al. 1989), NiNW show clear length-dependent inflammogenicity in the peritoneal cavity, with L-NiNW being highly inflammogenic and S-NiNW not significantly inflammogenic.

The potential cause of this difference in response to long and short nanowires, which were otherwise chemically identical, can be sought in the handling of fibres by macrophages. Macrophages removed from the peritoneal cavity 24 h after injection of either the S-NiNW or NiNP showed complete engulfment of the particles which are localised to the cytoplasm. However, a proportion of macrophages removed after intraperitoneal injection of the L-NiNW sample show incomplete phagocytosis with fibre protruding from the cell or two macrophages sharing a single fibre which causes both macrophages to undergo frustrated phagocytosis. Frustrated phagocytosis is accompanied by release of cellular components involved in microbiocidal activity such as NADPH oxidase-dependent release of reactive oxidant species (ROS) (Hansen & Mossman 1987), cytokines and release of proteases and other components of cytoplasmic lysosomes. This may cause further recruitment of inflammatory cells as well as 'innocent bystander' injury to the surrounding mesothelium (Kamp et al. 1992; Ye et al. 1999). Indeed, within our experiments, an increase in the lavage cytokine IL-6 was noted in the peritoneal cavity after injection of L-NiNW. In order to provide clearer information of the effect of long fibres on macrophages, we used an *in vitro* system in which the NiNW were incubated with macrophages. The results showed internalisation of the shorter fibres and similar protrusions of the long

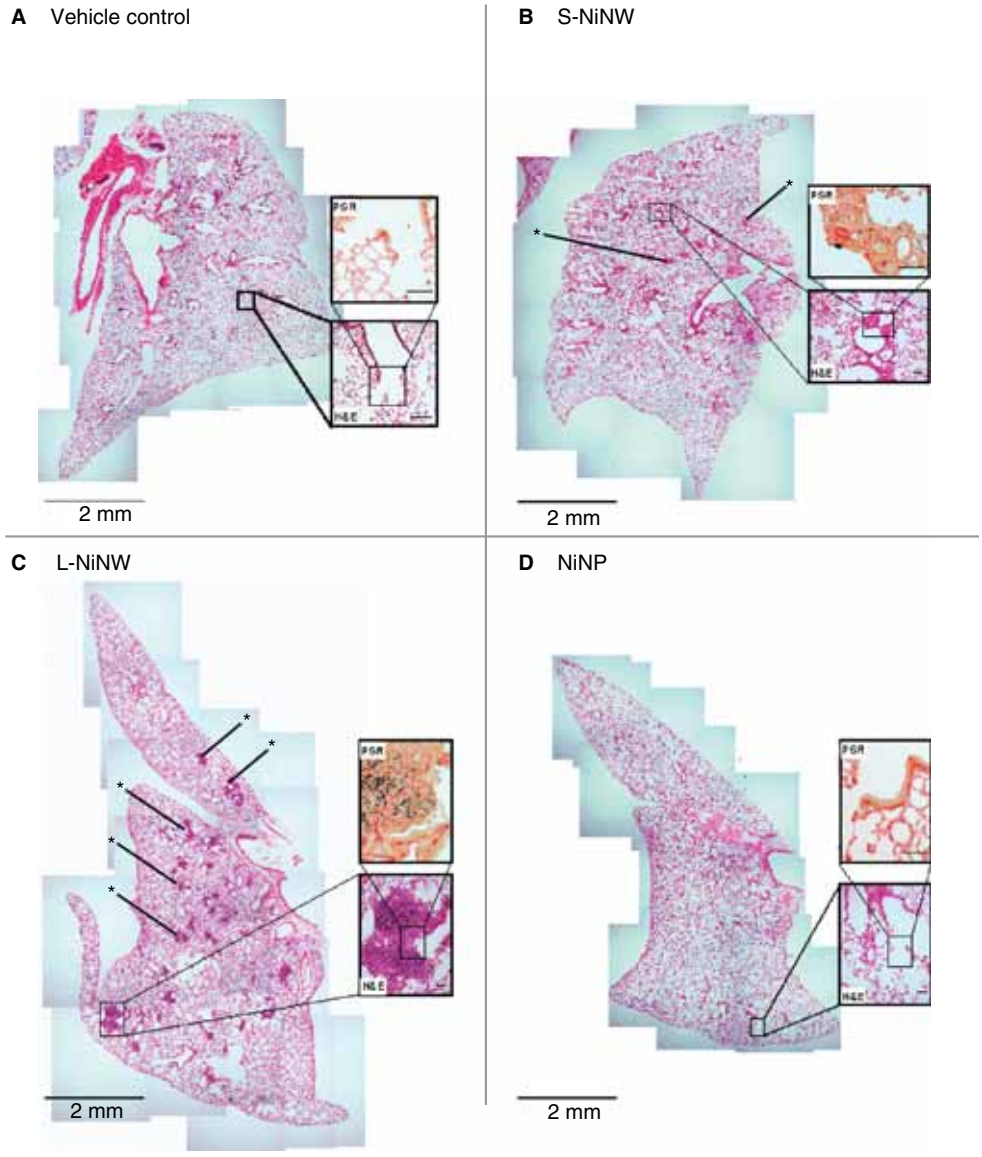

Figure 7. Lung pathology 7 days post aspiration with particles. The effect of different lengths of nickel nanowire samples and nickel nanoparticles is demonstrated 7 days after 50 μg aspiration of each test sample into the lungs of C57BL/6 mice. Each panel shows an entire lung section stained with haematoxylin & eosin (H&E) stain to demonstrate gross pathology with call-outs showing high magnification (×1000) terminal bronchioles. These call-outs show the same stained with H&E and Pico-Sirius Red (PSR) to show collagen deposition (red stain). Asterisks denote the presence of representative collagenous granulomas. Lung images taken at ×25 and call-outs at ×1000 magnification. Treatments performed $N = 3$ and vehicle control $N = 2$.

fibres out of the cells as seen *in vivo*. The same length-dependent effects for IL-1β and IL-6 were also noted which suggests that IL-1β and IL-6 are involved in the length-dependent inflammation in the peritoneal cavity *in vivo* whilst TNF-α and CCL3 may not. The findings that NiNP stimulated the release of TNF-α and CCL3 by NiNP *in vitro* is somewhat puzzling but may relate to the release of soluble nickel from the NINP driving a reaction due to its large surface area. Indeed, the ability of soluble nickel to drive an allergic type reaction resulting in high TNF-α levels after exposure has been shown in humans (Möller et al. 1999) and *in vitro* (Cortijo et al. 2010) although in the latter it also caused an increase in IL-1β in a type II alveolar epithelial cell line (A549). Indeed, it has previously been reported that there can be dramatic differences in the ability of particles to stimulate TNF-α and IL-1β, e.g., with silica there was a 10 times greater IL-1β response than TNF-α in the NR8383 macrophage cell line (Liu et al. 2007) whilst environmental particles caused more than 10-fold greater TNF-α than IL-1β response in human alveolar macrophages in culture (Ishii et al. 2004). Differences in signalling pathways for the two cytokines may account for these differences along with differences in particle stress effects on cells in culture, e.g., oxidative stress versus direct membrane damage. However, the importance of these data lie in their ability relevance as an indicator for a predictive *in vitro* assay for length-dependent effects although clearly further work is needed.

In relation to the ability of NiNP to stimulate TNF-α and CCL3 production, it may be the case that such

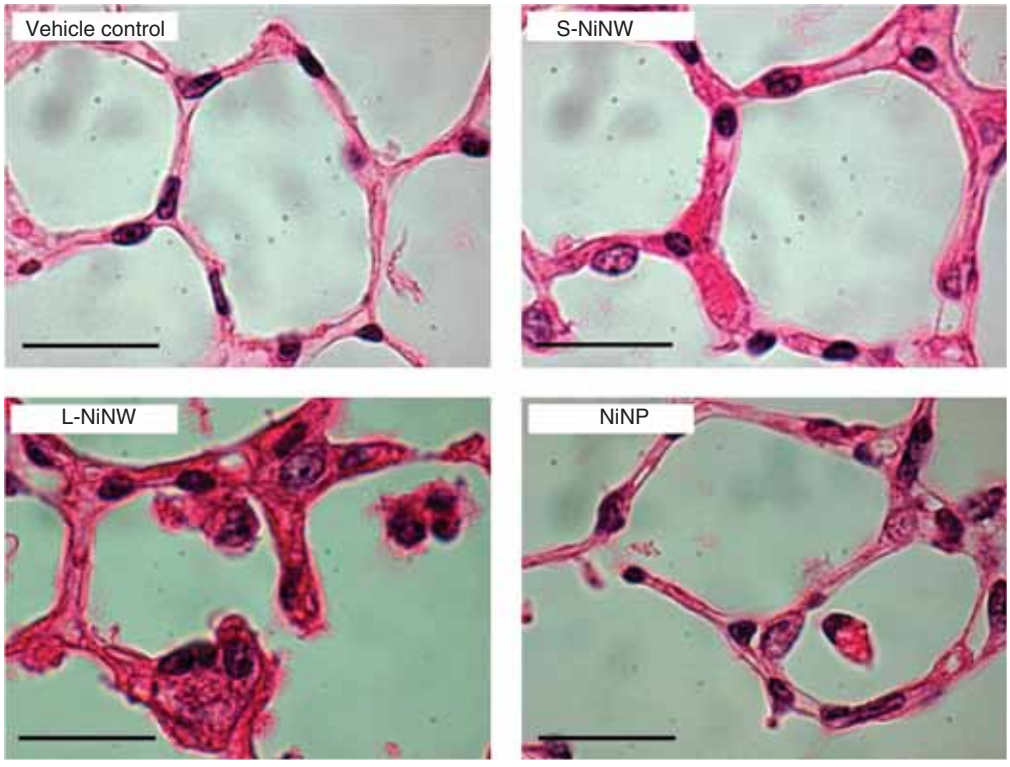

Figure 8. Lung alveolar septa 7 days post aspiration of nickel particles. The effect of lung aspiration of different lengths of nickel nanowires and nickel nanoparticles on the alveolar septa is shown 7 days after aspiration of each test sample into the lungs of mice. The images for each are stained with H&E stain and taken at ×1000 magnification at roughly equidistance from the terminal bronchioles; scale bar = 20 μm. Treatments performed $N = 3$ and vehicle control $N = 2$.

pro-inflammatory reactivity may drive the airway neutrophilia we saw in the lungs and BAL of mice treated with NiNP. When considering the mesothelial response as a surrogate for the pleural response, prolonged contact with nickel particles of small dimensions is unlikely to happen due to rapid clearance routes from mesothelial cavities as previously discussed, resulting in a removal of dose. IL-1β activation through cleavage by caspase-1 and subsequent secretion may occur due to frustration of phagocytosis by the retained L-NiNW leading to ROS generation via NADPH oxidase activation. This in turn can lead to activation of the Nalp3 inflammasome resulting in activation of caspase-1 and secretion of IL-1β (Dostert et al. 2008; Cassel et al. 2008), which was not seen with the low-aspect ratio nickel nanowires (S-NiNW) and nanoparticles (NiNP) which did not hinder uptake. The secretion of IL-1β via inflammasome mediated pathway may in turn lead to the corresponding increase in IL-6 which is not inflammasome-dependent whose expression can be activated by IL-1β (Zhang et al. 1990); however, this does not explain why secretion of TNF-α did not also lead to an increase in IL-6 via nuclear factor kappa-B activation.

Within the lung, normal pulmonary clearance ensures that most of the particles that reach the distal lung are removed upwards by macrophages and mucocillary action and never reach the pleural or peritoneal mesothelium. However, we recently reviewed the data (Donaldson et al. 2010) supporting the contention that a proportion of all deposited particles and fibres pass through from the lung into the pleural space (Mitchev et al. 2002; Muller et al. 2002). The normal elutriating effects of passage through the airways ensures that peripherally-depositing particles are all small (<5 μm aerodynamic diameter (D_{ae})) and so those that do reach the pleura can easily exit through the stomatal pores in the parietal pleura which are around 3–12 μm (Mutsaers 2002) and enter the lymphatic system. We suggest that long fibres, which can still reach the distal lungs and pleura, because of their uniquely small D_{ae} despite their length, cannot negotiate these stomata and build up on the parietal pleura leading to disease (Donaldson et al. 2010). Thus, the pleural space has a size-selective mechanism of clearance that has an analogous size-dependent mechanism in the peritoneal cavity making the mouse peritoneal assay a realistic model for studying fibre length effects that occur primarily in the pleural cavity, with obvious caveats. These include the fact that the space between the parietal and visceral pleura is notional, only around 20–50 μm, and fluid filled with a constantly moving apposing surfaces. However, the fibre length-dependent inflammatory response in the peritoneal and pleural spaces is similar with CNT although the response to L-NiNW waned with time in the peritoneal cavity, as seen with CNT and long fibre amosite asbestos, whereas over a week the inflammation persists in the pleural space (Murphy et al. 2011).

A length-dependent difference was also seen within the lung after aspiration of the nickel nanowires and particles as assessed at the later time point of 7 days for the purpose of assessing the pathology. This difference in the pathological

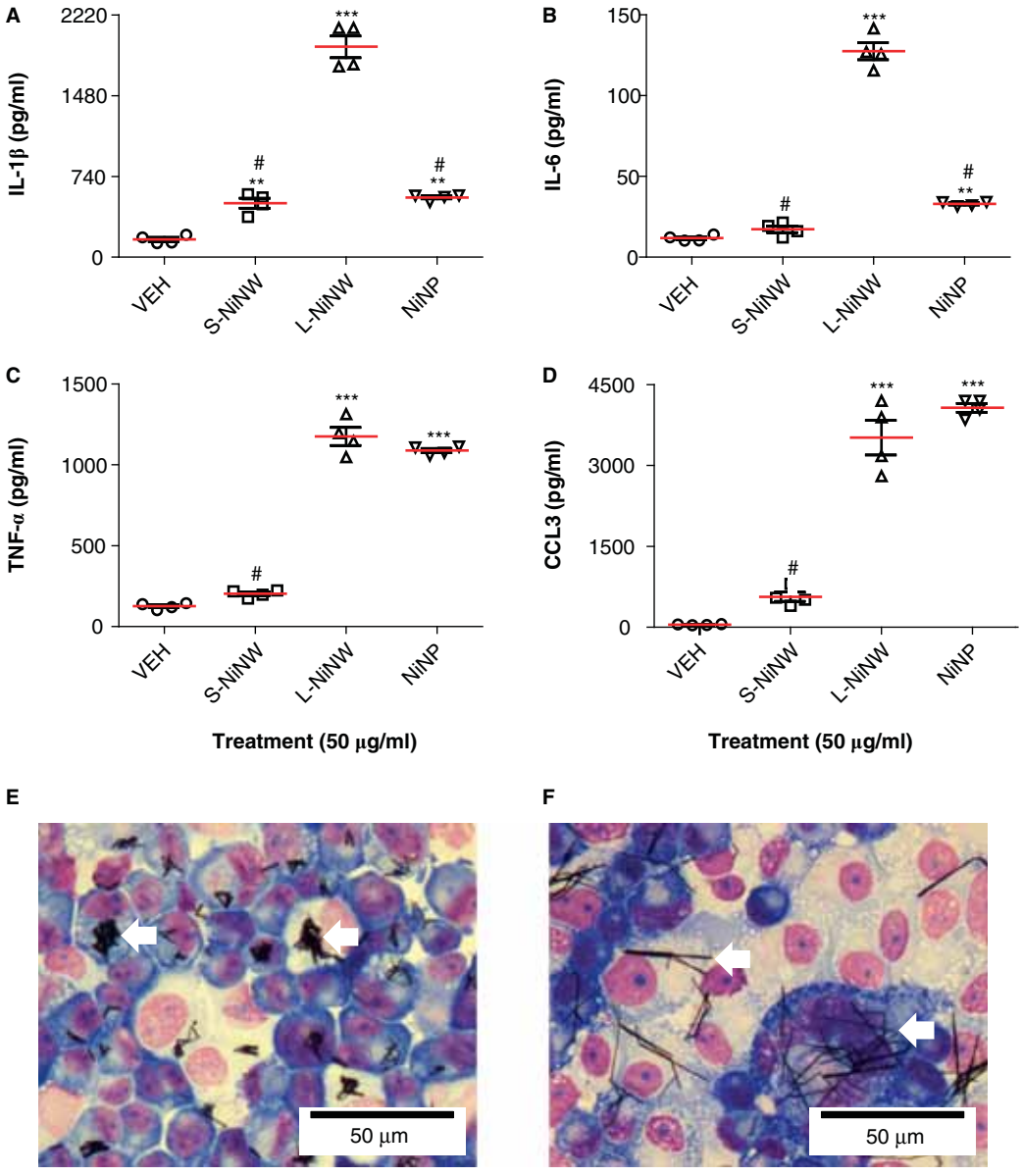

Figure 9. THP-1 inflammatory response to nickel nanowires. Differentiated THP-1 macrophages were treated with 5 μg/ml of long and short nickel nanowires (S-NiNW and L-NiNW, respectively) and nickel nanoparticles (NiNP). After 24 h the media were aspirated and analysed for secretion of the acute phase response cytokines (A) interleukin-1β (IL-1β), (B) interleukin-6 (IL-6), (C) tumour necrosis factor-alpha (TNF-α) and (D) the chemokine CCL3 (MIP-1α). A cytocentrifugation preparation stained with Diff Quik was made of the treated cells to show cellular uptake of S-NiNW (E) and L-NiNW (F). Scatter plot with mean of four experiments ± s.e.m. Significance vs. vehicle control indicated by $^{**}p < 0.01$, $^{***}p < 0.001$ and vs. L-NiNW $^{\#}p < 0.001$. All images were taken at ×1000 magnification.

response was not as marked between the long and short fibres as seen in the peritoneal cavity reflecting the difference in structure of these two areas and possibly tempo of inflammatory response. The nature of an instilled particle dose into the lung associated with aspiration (as opposed to inhalation) is that the dose rate is substantial, i.e., instantaneous delivery of dose, meaning that the initial response is intense and then clearance processes come into play and the inflammation wanes. However, in comparison to the peritoneal cavity, the clearance rate in the lung is likely to be slower resulting in a longer retention of dose of leading to some associated effects with small particles (e.g., as seen with the NiNP). Within the peritoneal cavity and most likely within the pleural cavity where clearance routes are similar, the outflow of small particles via the diaphragmatic stomata to outlying lymph nodes is very rapid (in contrast to long fibres which cannot negotiate the stomata) meaning a dose is not retained over a sufficient period of time to elicit any form of pathology. Indeed, when comparing the pathology of the two locations, we see that aspiration of spherical NiNP into the lungs led to alveolar deposition and diffuse alveolitis at 7 days but did not appear to affect terminal bronchioles or alveolar duct bifurcations. In contrast, the long fibres generated numerous granulomas associated with fibres and showed prominent collagen deposition. The frequent occurrence of these granulomas at terminal bronchioles and alveolar ducts is well described (Brody et al. 1984) and is the result of interception of the long fibres at this narrowing. The resultant frustrated phagocytosis may mean that macrophages are unable to clear the long fibres to the ciliated

epithelium of the terminal bronchiole and so the granuloma evolves around the retained fibres. Within the early granulomas, the pro-inflammatory effects of frustrated phagocytosis of the long fibres likely leads to further cellular recruitment at the site of deposition, leading to granuloma enlargement and blocking of the airspaces. This process was seen to a much lesser extent after aspiration of S-NiNW but none the less, occasional granulomas were present at terminal bronchioles and alveolar ducts. To sum up, despite the same chemical composition, differing morphology of the nickel samples has led to differential patterns of deposition and retention (first alveolar duct bifurcation vs. peripheral alveoli) and different cellular response (focal granuloma formation vs. mild diffuse alveolitis). The alveolitis seen within the L-NiNW treated animals may be an indirect result of the presence of substantial bronchiolar lesions rather than necessarily a direct interaction with L-NiNW. This is because whilst the alveolitis was extensive, the presence of particles was more focal within the lesions at the terminal bronchioles (although some fibres were noted in the distal alveolar regions).

In their seminal 1981 paper (Stanton et al. 1981), Stanton and colleagues discussed the results of 72 experiments whereby respirable durable minerals of various sizes were implanted into the pleurae of rats. The resultant malignant mesenchymal neoplasms were recorded and the data analysed for correlation between the particle dimensions and the ensuing neoplasms. They found that the probability of developing such pleural pathology correlated best with fibres that were 8 μm in length and 0.25 μm in diameter, concluding overall that due to the wide variety of compounds tested, the carcinogenicity of fibres was dependent on dimension and durability. In conclusion, our data presented herein show that like asbestos and CNTs, NiNW show length-dependent inflammogenicity in the mouse peritoneal cavity. In addition when instilled into the lung, long fibres were retained in the centri-acinar region following deposition, causing granulomas and inflammation, whilst the S-NiNW and NiNP had little effect beyond mild alveolar inflammation. The response to L-NiNW was not driven by the chemical structure or soluble components as nickel in other, compact forms did not induce a reaction nor did an aqueous extract. This lends support to the contention that the FPP is applicable to HARNs generally where they meet the criteria outlined in the FPP (long, thin biopersistent). Whilst our experimental data allow further confirmation of the role of length in fibre toxicity based on broad size classes, further work is required to truly define at what length a fibre becomes pathogenic.

There is concern that the production and use of NPs on an industrial scale could lead to exposure and adverse health effects in workers and the general population (The Royal Society and Royal Academy of Engineering 2004; Maynard et al. 2006; The Economist 2007). The success of the nanotechnology industry depends on public acceptance, regulatory compliance and acceptable risk. There is a considerable need to supply hazard data, both quantitative and qualitative, for the risk assessment process. The data shown here confirm our findings with CNTs and suggest the real possibility that all nanofibres will conform to the FPP. The UK Health and Safety Executive has taken steps to produce guidelines on the risk management of CNT (The Health and Safety Executive 2009) highlighting the importance of fibre length and applicability of their guidelines to other biopersistent nano-dimensioned fibres (HARN) and the need to characterise airborne nanofibres in order to properly assess the risk to the workers. Using the FPP as a basis for designing 'safe' HARN suggests that short or non-biopersistent long HARN should be the goal.

Acknowledgements

The authors gratefully acknowledge financial support from the Colt Foundation, the help of Dr. Robert Morris for histological assistance and Mr. Steven Mitchell for his electron microscopy expertise. This work was partly supported by the European Commission FP7 NAMDIATREAM (NMP-2009-246479) research project (F.B., A.P.M., Y.G., Y.V.) and Science Foundation Ireland as part of the MANSE (SFI-PI grant) and CRANN CSET funded facilities.

Declaration of interest

The authors report no conflicts of interest. The authors alone are responsible for the content and writing of the paper.

References

Brody AR, Warheit DB, Chang LY, Roe MW, George G, Hill LH. 1984. Initial deposition pattern of inhaled minerals and consequent pathogenic events at the alveolar level. Ann NY Acad Sci 428:108–120.

Brown DM, Stone V, Findlay P, MacNee W, Donaldson K. 2000. Increased inflammation and intracellular calcium caused by ultrafine carbon black is independent of transition metals or other soluble components. Occup Environ Med 57:685–691.

Byrne F, Prina-Mello A, Whelan A, Mohamed BM, Davies A, Gun'ko YK, et al. 2009. High content analysis of the biocompatibility of nickel nanowires. J Magnetism Magn Mater 321(10):1341–1345.

Cao G, Liu D. 2008. Template-based synthesis of nanorod, nanowire, and nanotube arrays. Adv Colloid Interface Sci 136(1-2):45–64.

Cassel SL, Eisenbarth SC, Iyer SS, Sadler JJ, Colegio OR, Tephly LA, et al. 2008. The Nalp3 inflammasome is essential for the development of silicosis. Proc Natl Acad Sci USA 105 (26):9035–9040.

Cho WS, Rodger Duffin R, Poland CA, Duschl A, Oostingh GJ, MacNee W, et al. 2011. Differential pro-inflammatory effects of metal oxide nanoparticles and their soluble ions in vitro and in vivo; zinc and copper nanoparticles, but not their ions, recruit eosinophils to the lungs. Nanotoxicology (early on-line February 18):1–14.

Cortijo J, Milara J, Mata M, Donet E, Gavara N, Peel SE, et al. 2010. Nickel induces intracellular calcium mobilization and pathophysiological responses in human cultured airway epithelial cells. Chem Biol Interact 183(1):25–33.

Donaldson K, Aitken R, Tran L, Stone V, Duffin R, Forrest G, Alexander A. 2006. Carbon nanotubes: a review of their properties in relation to pulmonary toxicology and workplace safety. Toxicol Sci 92(1):5–22.

Donaldson K, Brown GM, Brown DM, Bolton RE, Davis JM. 1989. Inflammation generating potential of long and short fibre amosite asbestos samples. Br J Ind Med 46(4):271–276.

Donaldson K, Murphy F, Duffin R, Poland C. 2010. Asbestos, carbon nanotubes and the pleural mesothelium: a review and the hypothesis regarding the role of long fibre retention in the parietal pleura, inflammation and mesothelioma. Part Fibre Toxicol 7(1):5.

Donaldson K. 2009. The inhalation toxicology of p-aramid fibrils. Crit Rev. Toxicol., 39(6): 487–500.

Dostert C, Petrilli V, Van BR, Steele C, Mossman BT, Tschopp J. 2008. Innate immune activation through Nalp3 inflammasome sensing of asbestos and silica. Science 320(5876):674–677.

Hansen K, Mossman BT. 1987. Generation of superoxide (O_2^-.) from alveolar macrophages exposed to asbestiform and nonfibrous particles. Cancer Res 47(6):1681–1686.

Ishii H, Fujii T, Hogg JC, Hayashi S, Mukae H, Vincent R, van Eeden SF. 2004. Contribution of IL-1 beta and TNF-alpha to the initiation of the peripheral lung response to atmospheric particulates (PM10). Am J Physiol Lung Cell Mol Physiol 287(1): L176–L183.

Julien C, Esperanza P, Bruno M, Alleman LY. 2011. Development of an in vitro method to estimate lung bioaccessibility of metals from atmospheric particles. J Environ Monit 13:621–630.

Kamp DW, Graceffa P, Pryor WA, Weitzman SA. 1992. The role of free radicals in asbestos-induced diseases. Free Radic Biol Med 12(4):293–315.

Knaapen A, Shi T, Borm PJA, Schins RPF. 2002. Soluble metals as well as the insoluble particle fraction are involved in cellular DNA damage induced by particulate matter. Mol Cell Biochem 234-235:317–326.

Knez M, Bittner AM, Boes F, Wege C, Jeske H, Mai[beta] E, Kern K. 2003. Biotemplate synthesis of 3-nm Nickel and Cobalt Nanowires. Nano Lettx 3(8):1079–1082.

Liu H, Zhang H, Forman HJ. 2007. Silica induces macrophage cytokines through phosphatidylcholine-specific phospholipase C with hydrogen peroxide. Am J Respir Cell Mol Biol 36(5):594–599.

Lu S, Duffin R, Poland C, Daly P, Murphy F, Drost E, et al. 2009. Efficacy of simple short-term in vitro assays for predicting the potential of metal oxide nanoparticles to cause pulmonary inflammation. Environ Health Perspect 117(2):241–247.

Maynard AD, Aitken RJ, Butz T, Colvin V, Donaldson K Oberdorster G, et al. 2006. Safe handling of nanotechnology. Nature 444(7117):267–269.

McNeilly JD, Heal MR, Beverland IJ, Howe A, Gibson MD, Hibbs LR, et al. 2004. Soluble transition metals cause the pro-inflammatory effects of welding fumes in vitro. Toxicol Appl Pharmacol 196(1):95–107.

Mitchev K, Dumortier P, De VP. 2002. 'Black Spots' and hyaline pleural plaques on the parietal pleura of 150 urban necropsy cases. Am J Surg Pathol 26(9):1198–1206.

Möller H, Ohlsson K, Linder C, Björkner B, Bruze M. 1999. The flare-up reactions after systemic provocation in contact allergy to nickel and gold. Contact Dermatitis 40(4):200–204.

Muller KM, Schmitz I, Konstantinidis K. 2002. Black spots of the parietal pleura: morphology and formal pathogenesis. Respiration 69(3):261–267.

Murphy F, Duffin R, Poland CA, Al–Jamal KT, Ali-Boucetta H, Nunes A, et al. 2011. Length dependent retention of carbon nanotubes in the pleural space of mice initiates sustained inflammation and progressive fibrosis on the parietal pleura. Am J Pathol 178 (6):2587–2600.

Mutsaers SE. 2002. Mesothelial cells: their structure, function and role in serosal repair. Respirology 7(3):171–191.

Nel AE, Diaz-Sanchez D, Li N. 2001. The role of particulate pollutants in pulmonary inflammation and asthma: evidence for the involvement of organic chemicals and oxidative stress. Curr Opin Pulm Med 7(1):20–26.

Poland CA, Duffin R, Kinloch IA, Maynard AD, Wallace WA, Seaton A, et al. 2008. Carbon nanotubes introduced into the abdominal cavity of mice show asbestos-like pathogenicity in a pilot study. Nat Nanotechnol 3(7):423-428.

Pott F, Ziem U, Reiffer FJ, Huth F, Ernst H, Mohr U. 1987. Carcinogenicity studies in fibres, metal compounds, and some other dusts in rats. Exp Pathol 32:129–152.

Prina-Mello A, Diao Z, Coey JM. 2006. Internalization of ferromagnetic nanowires by different living cells. J Nanobiotechnol 4:9.

Rao GV, Tinkle S, Weissman DN, Antonini JM, Kashon ML, Salmen R, et al. 2003. Efficacy of a technique for exposing the mouse lung to particles aspirated from the pharynx. J Toxicol Environ Health A 66(15):1441–1452.

Service RF. 1998. CHEMISTRY: nanotubes: the next asbestos? Science 281(5379):941.

Stanton MF, Layard M, Tegeris A, Miller E, May M, Morgan E, Smith A. 1981. Relation of particle dimension to carcinogenicity in amphibole asbestosis and other fibrous minerals. J Natl Cancer Inst 67:965–975.

The Health and Safety Executive. Risk management of carbon nanotubes. 2009.

The risk in nanotechnology: a little risky business. The Economist Nov 22 2007. 2007.

The Royal Society and Royal Academy of Engineering. Nanoscience and nanotechnologies: opportunities and uncertainties. The Royal Society. 29-7-2004.

Ye J, Shi X, Jones W, Rojanasakul Y, Cheng N, Schwegler-Berry D, et al. 1999. Critical role of glass fiber length in TNF-alpha production and transcription factor activation in macrophages. Am J Physiol 276 (3 Pt 1):L426-L434.

Zhang YH, Lin JX, Vilcek J. 1990. Interleukin-6 induction by tumor necrosis factor and interleukin-1 in human fibroblasts involves activation of a nuclear factor binding to a kappa B-like sequence. Mol Cell Biol 10(7):3818–3823.

Zhou JC, Gao Y, Martinez-Molares AA, Jing X, Yan D, Lau J, et al. 2008. Microtubule-based gold nanowires and nanowire arrays. Small 4 (9):1507–1515.

Supplementary material available online

Appendix.

Supporting Information Available

Within the appendix section the results of the soluble extract of long nickel nanowires injected into the peritoneal cavity, the total polymorphonuclear neutrophil (PMN) results within the BAL fluid post lung instillation of the nickel particles and the results of the total lavagable cells and total lavagable PMN can be found.